

CARI4D: Category Agnostic 4D Reconstruction of Human-Object Interaction

Xianghui Xie^{1,2,3,4,*}Bowen Wen^{1,✉}Yan Chang¹Hesam Rabeti¹Jiefeng Li¹Ye Yuan¹Gerard Pons-Moll^{2,3,4}Stan Birchfield¹¹NVIDIA ²University of Tübingen ³Tübingen AI Center ⁴Max Planck Institute for Informatics

*Work done during internship at NVIDIA ✉ Corresponding author

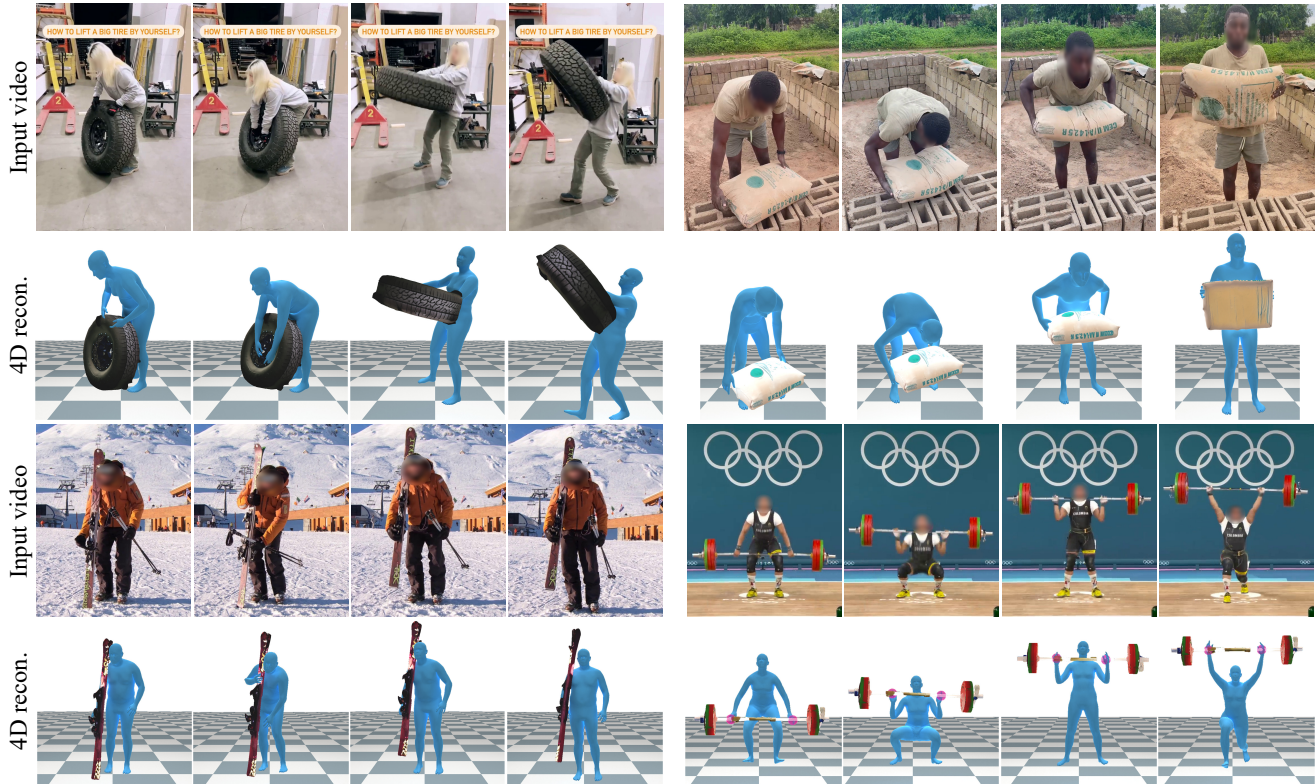


Figure 1. **Results on in-the-wild internet videos.** Given a monocular RGB video, CARI4D reconstructs the human and object at metric scale, and tracks the 4D human-object interaction consistently across the video. Our method is category agnostic and generalizes zero-shot.

Abstract

Accurate capture of human-object interaction from ubiquitous sensors like RGB cameras is important for applications in human understanding, gaming, and robot learning. However, inferring 4D interactions from a single RGB view is highly challenging due to the unknown object and human information, depth ambiguity, occlusion, and complex motion, which hinder consistent 3D and temporal reconstruction. Previous methods simplify the setup by assuming ground truth object template or constraining to a limited set of object categories. We present CARI4D, the first category-

agnostic method that reconstructs spatially and temporarily consistent 4D human-object interaction at metric scale from monocular RGB videos. To this end, we propose a pose hypothesis selection algorithm that robustly integrates the individual predictions from foundation models, jointly refine them through a learned render-and-compare paradigm to ensure spatial, temporal and pixel alignment, and finally reasoning about intricate contacts for further refinement satisfying physical constraints. Experiments show that our method outperforms prior art by 38% on in-distribution dataset and 36% on unseen dataset in terms of reconstruction error. Our model generalizes beyond the training cat-

egories and thus can be applied zero-shot to in-the-wild internet videos. Our code and pretrained models will be publicly released.

1. Introduction

Traditionally, capturing human-object interaction requires tedious and expensive setups, such as special studios or multi-view camera arrays [6, 9, 22]. While such approaches have been used in various applications (movies, gaming, robotics, augmented / virtual reality, etc.), their impact has been limited because they do not scale.

Monocular RGB videos, on the other hand, are not only abundantly available online, but new data can be captured quickly and affordably. As a result, approaches that can extract 4D human-object interactions directly from monocular RGB videos are highly desirable. Reconstruction from RGB alone, however, introduces several challenges: (1) Both the human and object shape and pose can vary significantly between different subjects or categories; (2) The lack of depth information makes it difficult to recover scale and detailed geometry; and (3) The model needs to reason about shape, scale, pose, and dynamics while being robust to heavy occlusions.

To overcome these challenges, prior works on human-object reconstruction rely on ground truth object templates to train an instance-specific pose estimator [55], or they assume the categories are known beforehand, training models that do not generalize beyond the categories covered by the training data [56, 57]. More recent image-based reconstruction work [10] handles more categories by constructing databases of human-object contacts in the wild. While showing impressive results, contact retrieval is still limited to the annotated categories, and translations are inconsistent across video frames.

In this paper, we propose a method for **Category Agnostic 4D Reconstruction of human-object Interaction (CARI4D)** to address these limitations. Our design bridges research and real-world usage by (1) reconstructing objects directly from input without pre-defined models, (2) generalizing beyond fixed categories, and (3) maintaining consistent metric reconstruction and tracking across video frames.

To solve this challenging problem, we start with existing foundation models. Such models have shown impressive generalization on tasks like shape reconstruction [40, 53, 60, 61], pose estimation [23, 36, 50] and scene understanding [5, 31, 46]. However, combining them is non-trivial, because their predictions lie in different coordinate spaces, they suffer from noisy input, and they do not consider the fine-grained contacts important for interaction. Our key idea is to carefully align the predictions from foundation models to obtain robust metric initialization, followed by an interaction-specific model that is trained to reason about

contacts, which are used to further refine the interaction poses through joint optimization.

Specifically, we propose a coarse-to-fine scale estimation strategy for metric object shape reconstruction. A novel pose hypothesis selection algorithm is then used to robustly track object pose under heavy occlusion. We also adopt foundation models to obtain human pose estimations that are aligned to the same depth and scale as the object. To refine these foundation model initializations, we introduce **CoCoNet**, a **Category agnostic Contact** reasoning model that renders the initial human-object estimations and compares with input observations to predict delta pose updates together with contacts. These poses and contacts are then sent into a contact-aware joint optimization framework to obtain coherent interactions.

In summary, our main contributions are:

- We present CARI4D, the first category-agnostic method that reconstructs the object at metric scale and tracks the 4D human-object interaction with consistent translation and contacts, all from a single RGB video input.
- We propose several novelties: (1) A pose hypothesis selection algorithm that robustly tracks object pose under occlusions; (2) CoCoNet, a category-agnostic contact reasoning network that refines human and object poses using a render and compare paradigm; and (3) a contact-aware joint optimization framework.
- When trained on two real-world datasets, our method outperforms baselines by more than 36% in terms of chamfer distance on both in-distribution and unseen datasets. Our method also generalizes to in-the-wild videos where object categories are completely unseen.

Our code and pretrained models will be publicly released.

2. Related Works

Foundation models for 3D reasoning. There has been great progress in shape reconstruction [49, 53, 61], pose estimation [36, 50], scene understanding [45, 48] that reason 3D from monocular RGB cameras. High-quality object meshes with texture can be reconstructed from single image using direct 3D generation [40, 41, 53, 74] or multi-view image diffusion models [43, 59, 60]. Given an object mesh, FoundationPose [50] can estimate and track the object pose consistently in an RGBD video. Similarly, recent works have enabled high-quality human avatar creation from a single image [20, 61], monocular RGB videos [14, 15], or text [62]. Large scale datasets [4, 21, 29] also allow training foundation models for human pose estimation [7, 13, 23, 36] that generalizes well to in-the-wild videos. For scene understanding, recent works have pushed the boundary from relative depth [34, 46, 47, 65] towards metric-scale depth [5, 8, 31, 32] estimation and shown impressive generalization to both indoor and outdoor environments. While making significant progress, these models

treat human, object, and the environment separately and do not consider their intricate interactions.

Image-based interaction reconstruction. Joint hand-object reconstruction has been studied for decades, with works tackling the problem with synthetic data generation [16], temporal photometric consistency [17], contact potential field [64], or diffusion priors [66, 67]. For full body interaction, early works [52, 73] are optimization based and follow up works propose to learn from data using distance field [54], point cloud diffusion [56], or contact transformer [27]. Diverse interaction datasets and benchmark [58] with full 3D annotation [3, 18, 70, 75] or contact labels [10, 11, 24, 42, 71] are the driving force for this field. Recent efforts have pushed toward in-the-wild reconstruction for arbitrary objects [10, 11, 19, 51] or arbitrary scenes [63]. Although image-based methods demonstrate impressive generalization, they often produce temporally inconsistent results, thereby hindering downstream tasks such as robotic learning.

Video-based interaction tracking. Most prior works assume a known object template and focus on tracking the human and object poses. Early works track the human and object pose from multi-view RGBD [3] or RGB [39] cameras, and RobustFusion [38] reduces the setup to a monocular RGBD camera. More recent work, VisTracker [55], attempts to track from monocular RGB video and handles occlusion using motion infilling. Leveraging a shape reconstruction model, InterTrack [57] can reconstruct and track the shape and pose within the trained categories. While showing strong generalization, none of these works can generalize zero-shot to unseen categories. For hand object interaction, HOLD [12] and Diff-HOI [66] are category agnostic but cannot handle large objects or heavy occlusions. Ours is the first method for full body interaction, and it generalizes zero-shot to in-the-wild videos.

3. Method

We introduce CARI4D, the first category-agnostic method to reconstruct 4D human object interaction from monocular RGB video. This is a highly challenging problem due to unknown object shape, depth-scale ambiguity, dynamic motion, and severe occlusions introduced by interaction. Foundation models for shape, pose, and scene reconstruction provide strong priors yet individual predictions do not align and can suffer from noisy input. Our key idea is to design a framework that integrates the predictions to obtain a robust initialization and then design a category agnostic interaction reasoning module to improve contact coherency.

Specifically, given a sequence of N RGB images $\{\mathbf{I}_i\}_{i=1}^N$ where a person interacts with an object, our goal is to reconstruct the object mesh \mathbf{O} with corresponding per-frame 6DoF poses $\{\mathcal{O}_i\}_{i=1}^N$, here $\mathcal{O}_i = (\mathbf{R}^o, \mathbf{t}^o)$ consists of rotation $\mathbf{R}^o \in SO(3)$ and translation $\mathbf{t}^o \in \mathbb{R}^3$. For the human,

we use the SMPL-H body model [25, 35] and estimate per-frame parameters $\{\mathcal{H}_i\}_{i=1}^N$, where $\mathcal{H}_i = (\boldsymbol{\theta}, \beta, \mathbf{t}^h)$ consists of the SMPL body pose $\boldsymbol{\theta}$, shape β and global translation \mathbf{t}^h parameters. Note that we reconstruct the human and object at *metric scale* with consistent *global translations* as this is important for downstream applications.

In this section, we will first discuss how to obtain object reconstruction at metric scale (Sec. 3.1) and initial pose estimation (Sec. 3.2) using foundation models. We then introduce our CoCoNet (Sec. 3.3) to refine interaction and predict contacts, which is used to obtain more faithful interaction via joint optimization (Sec. 3.4). An overview of our method can be found in Figure 2.

3.1. Metric-scale Object Reconstruction

We assume that the object is mostly visible in the first frame of the video. This is common during video recordings where the human stands beside the object before actual interaction. We hence use the first frame to obtain the object reconstruction and metric scale. Specifically, we use f-BRS [37] to obtain object mask and run Hunyuan3D-2 [40] to reconstruct the object mesh. Hunyuan3D produces reasonable object mesh yet at normalized scale in its local coordinate system with unsolved pose w.r.t. the camera. However, we aim at obtaining metric scale 4D reconstruction. To this end, we estimate metric depth using UniDepth [31, 32] and adopt FoundationPose [50] to estimate the scale using grid search in a coarse-to-fine manner. Given a list of predefined candidate scales, we run FoundationPose to estimate the 6DoF pose for each rescaled mesh using depth and intrinsics estimated by UniDepth. We rank the candidates based on the unidirectional chamfer distance from segmented object point cloud to the mesh under the sampled scale and transformed by the estimated 6DoF pose. We then pick the top-3 scales, uniformly sample ten scales within $(0.8s_{\min}, 1.2s_{\max})$ to perform a more fine-grained scale search. The scale with minimum chamfer distance is used to resize the initial Hunyuan3D mesh which becomes our metric object reconstruction \mathbf{O} .

3.2. Human and Object Pose Initialization

Leveraging foundation models [32, 36, 50], we obtain robust initialization of human and object pose estimations that are aligned in metric-scale space.

Using the metric-scale object mesh from Sec. 3.1, one can perform depth estimation with UniDepth [32] and solve per-frame object poses via FoundationPose [50]. However, FoundationPose assumes depth from a sensor and a known textured mesh. Directly applying it with estimated depth is unreliable due to noisy depth estimation, imperfect Hunyuan3D meshes, and occlusions during interactions. To address this, we introduce a pose hypothesis selection algorithm to improve FoundationPose results in our challenging

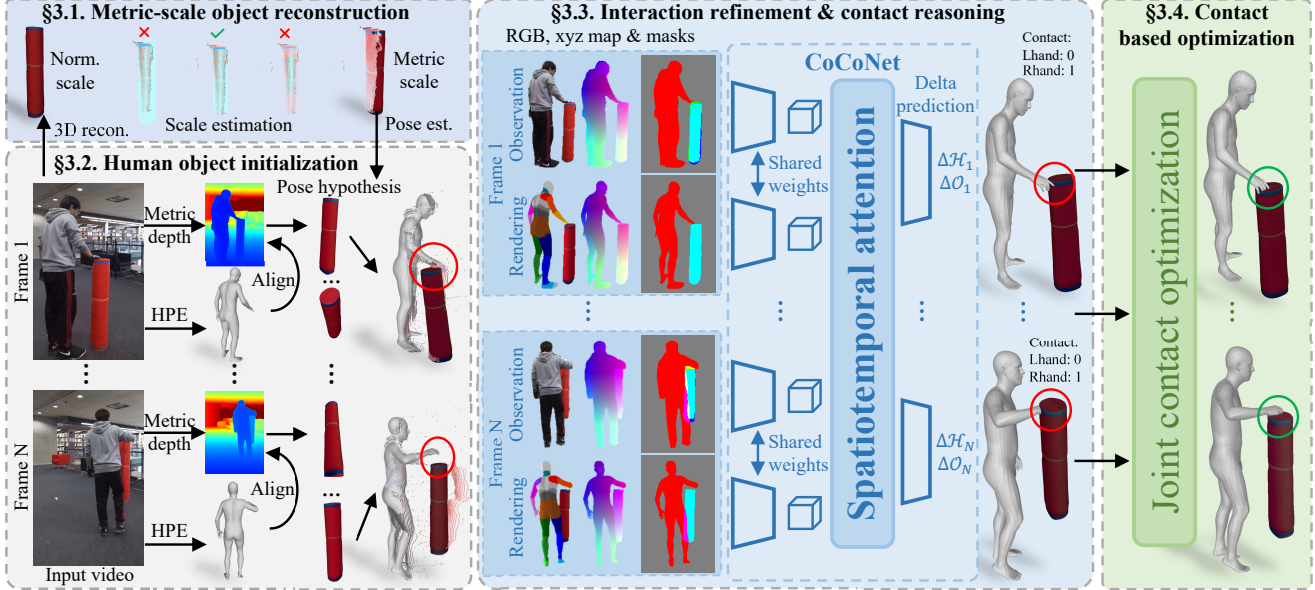


Figure 2. **CARI4D method overview.** Given a monocular RGB video, we reconstruct the 4D human and object at metric scale with consistent contacts. We start by estimating the metric-scale object mesh (Sec. 3.1), followed by initialization of human and object poses using dynamic pose hypothesis selection (Sec. 3.2). We then train a category agnostic contact reasoning model (CoCoNet) to refine the interaction poses and estimate hand contacts (Sec. 3.3) which are used to perform contact aware joint optimization (Sec. 3.4).

setup, producing more consistent per-frame object pose initialization for subsequent steps.

Object pose hypothesis selection. FoundationPose internally produces K pose candidates and their quality scores per frame, selecting the pose with the highest score as the output. In our considered more challenging setup, its top-1 prediction often fails, though the correct pose typically lies within the K candidates. Our key idea is to dynamically select the optimal pose per frame by leveraging visual cues and temporal consistency. Specifically, given object pose \hat{O}_{i-1} at previous frame $i-1$, our goal is to select the best pose from a list of pose hypothesis $\{\hat{O}_i^j\}_{j=1}^K$ (ranked from best to worst by FoundationPose) for current frame i . We consider two criteria to filter out wrong poses: a). **mask IoU** and b). **temporal smoothness**.

For **mask IoU**, we render each pose candidate \hat{O}_i^j into 2D mask M_i^j and compare with object mask M_i^o from input image. We subtract the input human mask M_i^h to take occlusion into account and define the IoU as: $\text{IoU}_i^j = \frac{\sum \tilde{M}_i^j \cap \tilde{M}_i^o}{\sum \tilde{M}_i^j \cup \tilde{M}_i^o}$, where $\tilde{M}_i^o = M_i^o \cap (\sim M_i^h)$, $\tilde{M}_i^j = M_i^j \cap (\sim M_i^h)$ and \sim denotes mask inversion. We filter out poses whose IoU is smaller than a threshold δ_m . For **temporal smoothness**, we compute the geodesic distance between candidate rotation \hat{R}_i^j and previous rotation \hat{R}_{i-1} and filter out poses whose distance is larger than a threshold δ_R . We apply IoU filter δ_m and temporal filter δ_R on the K pose candidates and the first one in the filtered list is the final object pose. This selection can sometimes filter out all poses due to occlusion or missing depth. In this case, we skip S

frames forward to a future frame where a good pose candidate can be found using criteria δ_m, δ_R and then run pose tracking and filtering backwards. We only apply filtering if pose candidates are left during backward pose tracking and multiple forward jumps are possible in case of long term occlusion. To further improve the robustness, we run FoundationPose in both RGB only (setting depth image to zeros) and RGBD mode to obtain the K pose candidates.

We show in Tab. 3 that this dynamic pose selection and forward-backward pose estimation obtains significantly better result than running vanilla FoundationPose.

Human estimation and alignment. For human, we run NLF [36] per-frame to obtain initial human pose estimations. NLF uses only RGB images, hence the predicted human may not align with the estimated metric depth from UniDepth [31] (to which object is aligned). We thus align NLF to the human depth predicted by UniDepth via optimizing the depth z and a global scale of NLF prediction in an iterative closest point manner.

3.3. Contact Reasoning and Refinement

While the pose estimations of human and object from Sec. 3.2 provides reasonable initialization, they are predicted separately and therefore do not reason about the fine-grained interactions. The object can be floating without contact, or penetrate with human due to noisy depth estimation or misaligned human depth, since the object and human have been treated independently in previous steps. We hence introduce **CoCoNet**, a **C**ategory agnostic **C**ontact reasoning model to refine the human and object jointly

while also estimating the intricate contacts.

Specifically, given initialized human and object poses $\{\hat{\mathcal{H}}_i, \hat{\mathcal{O}}_i\}_{i=1}^L$ from L input images (Sec. 3.2), our CoCoNet predicts the updated poses $\{\mathcal{H}_i, \mathcal{O}_i\}_{i=1}^L$ and binary contact labels $\{\mathbf{c}_i\}_{i=1}^L, \mathbf{c}_i \in \{0, 1\}^2$ indicating if each of the two hands is in contact with the object. Inspired by [50], we design our network in a render-and-compare paradigm together with spatial temporal attention to leverage jointly the initial 3D estimation, input visual observations and temporal cues. Given our reconstructed human and object mesh, we render under their initialized poses $\hat{\mathcal{H}}_i, \hat{\mathcal{O}}_i$ into RGB $\hat{\mathbf{I}}_i$, depth $\hat{\mathbf{D}}_i$, and human object masks $\hat{\mathbf{M}}_i$. We texture the SMPL mesh with distinct vertex colors for each body part for better semantic reasoning, as shown in Fig. 2 (middle). Our CoCoNet f_ϕ then consumes a sequence of renderings $\hat{\mathcal{T}} = \{\hat{\mathbf{I}}_i, \hat{\mathbf{D}}_i, \hat{\mathbf{M}}_i\}_{i=1}^L$ given the estimated pose parameters from the previous steps, and observations from the camera $\mathcal{I} = \{\mathbf{I}_i, \mathbf{D}_i, \mathbf{M}_i\}_{i=1}^L$ (\mathbf{D}_i and \mathbf{M}_i are obtained via off-the-shelf models), and predicts delta updates $\Delta\hat{\mathcal{H}}_i, \Delta\hat{\mathcal{O}}_i$ for each pose parameters together with the hand contact labels \mathbf{c}_i , formally: $f_\phi : (\hat{\mathcal{T}}(\hat{\mathcal{H}}_i, \hat{\mathcal{O}}_i), \mathcal{I}) \mapsto \{\Delta\hat{\mathcal{H}}_i, \Delta\hat{\mathcal{O}}_i, \mathbf{c}_i\}_{i=1}^L$. We use a frozen DINOv2 [28] encoder to extract the RGB features and a trainable lightweight DINOv2 encoder to extract features from masks \mathbf{M}_i stacked with 3D point map unprojected from the depth map \mathbf{D}_i . The encoders are shared between rendering $\hat{\mathcal{T}}_i$ and input images \mathcal{I}_i . We then apply a number of spatiotemporal attention [2] blocks on the extracted feature tokens and predict output using MLPs. Please refer to our Supp. for the detailed network.

Depth alignment for CoCoNet training. When curating the training data, our initial object poses are aligned to the predicted noisy depth [32] which deviate from the GT depth where GT poses are aligned to. Models trained naively with this mismatch tend to overfit to the error patterns of depth estimators instead of focusing on correcting the relative human-object poses. This is particularly problematic when training on multiple mixed datasets as the error patterns of metric-scale depth estimators change significantly across datasets. To this end, we propose to first align the estimated depth to GT depth, based on which, we then initialize human object poses. More specifically, we compute a scale s and shift t that align estimated depth \mathbf{D}^{pr} to GT depth \mathbf{D}^{gt} : $\mathbf{D}^{\text{align}} = s \cdot \mathbf{D}^{\text{pr}} + t$. Following MiDaS [34], we estimate s, t using medians $m^{\text{pr}}, m^{\text{gt}}$ of predicted and GT depth respectively:

$$s = \frac{\hat{s}^{\text{gt}}}{\hat{s}^{\text{pr}}}, \quad t = m^{\text{gt}} - s \cdot m^{\text{pr}}, \quad \text{where} \quad (1)$$

$$\hat{s}^{\text{pr}} = \frac{\sum_i |\mathbf{D}_i^{\text{pr}} - m^{\text{pr}}|}{\sum_i (\mathbf{D}_i^{\text{pr}} > 0)}, \quad \hat{s}^{\text{gt}} = \frac{\sum_i |\mathbf{D}_i^{\text{gt}} - m^{\text{gt}}|}{\sum_i (\mathbf{D}_i^{\text{gt}} > 0)}$$

To improve robustness, we apply erosion and bilateral filtering to both estimated and GT depth and consider only pixels within the human and object masks to compute s, t . We then

run FoundationPose and align the NLF prediction using the aligned depth maps. This alignment removes the absolute translation error from depth estimations and thus the network can focus on reasoning the relative poses between human and object. At test time, we do not perform any alignment to the estimated depth, since the network has learned to produce poses which are consistent with the given depth. This alignment reduces the learning efforts of our CoCoNet and improves reconstruction accuracy, see Tab. 3 d and e.

After alignment, we train our CoCoNet using standard L1 loss between predicted and ground truth variables for poses $\mathcal{H}_i, \mathcal{O}_i$, and binary cross entropy loss for the contacts \mathbf{c}_i . We also annotate the symmetric transformations for the object and apply symmetry loss [44] for the object pose predictions. Please refer to Supp. for more details.

3.4. Contact-based Joint Optimization

Our feedforward prediction from CoCoNet improves the relative pose between human and object, yet it cannot guarantee the contacts are satisfied and predictions are image aligned. We further improve the contact coherency and motion smoothness via contact aware joint optimization, guided by the contact predictions from Sec. 3.3. Specifically, we optimize the human and object pose parameters $\{\mathcal{H}_i, \mathcal{O}_i\}_{i=1}^N$ by minimizing the contact distances while satisfying visual constraints from input. The objective function is defined as:

$$L = \lambda_c L_c + \lambda_{j2d} L_{j2d} + \lambda_m L_m + \lambda_{\text{pen}} L_{\text{pen}} + \lambda_{\text{acc}} L_{\text{acc}} \quad (2)$$

where L_c is the contact loss that reduces the distance between human hands to the object when contacts are predicted: $L_c = \sum_i d(\mathbf{J}_i^h, \mathbf{O}'_i) \cdot \mathbf{c}_i$, where $d(\cdot, \cdot)$ computes the closest distance from two hand joints $\mathbf{J}_i^h \in \mathbb{R}^6$ to the posed object points \mathbf{O}'_i . We also leverage visual cues to define 2D projection loss L_{j2d} of SMPL body joints [54] and occlusion aware loss L_m for object masks [73]. We further constrain the optimization using penetration loss L_{pen} [26] and acceleration loss L_{acc} that encourages the acceleration to be zero. Exact loss definitions and weights λ_* are discussed in Supp.

4. Experiments

In this section, we compare our method with baselines and ablate our design choices. Results show that our method significantly outperforms all existing baselines on both in-distribution and unseen datasets. Ablation studies also validate the effectiveness of our proposed modules and our method generalizes zero-shot to in-the-wild videos. We discuss limitation and failure cases in supplementary.

Experiment Setup. We train our model on BEHAVE [3] and HODome [70] datasets. We preprocess the training data following Sec. 3.3 to align UniDepth [32], NLF [36], and FoundationPose [50] predictions to ground truth depth.

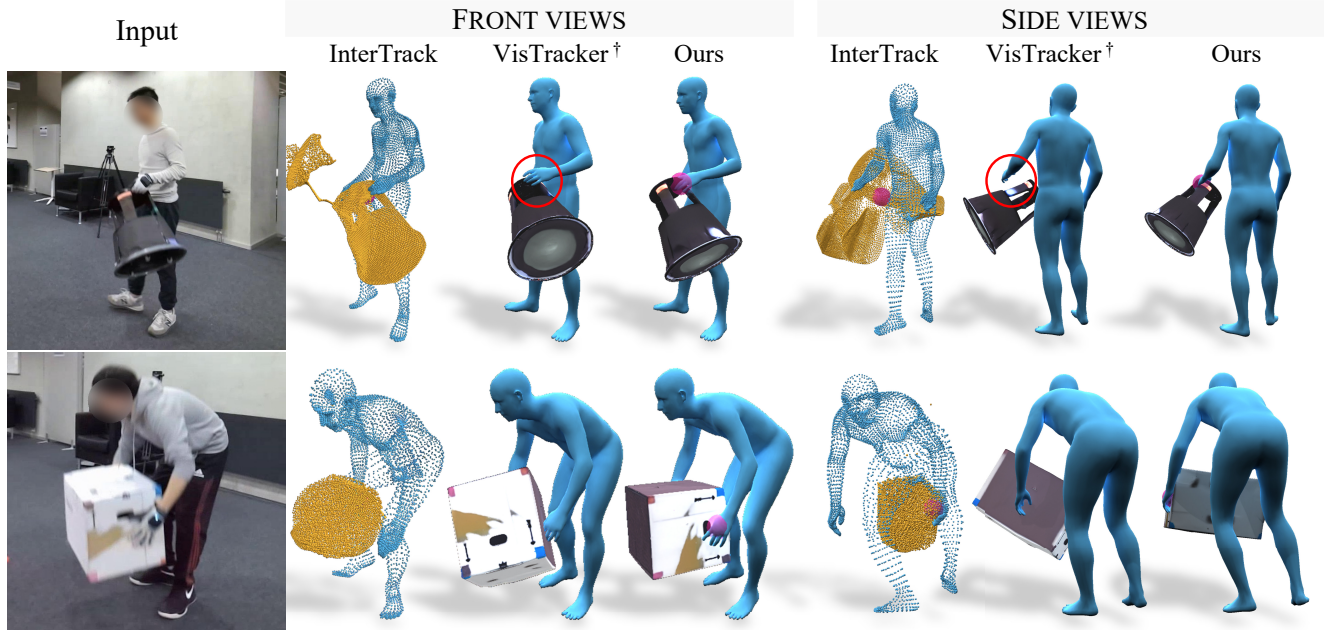


Figure 3. **Qualitative comparison on BEHAVE dataset** [3]. InterTrack [57] reconstructs human and object as point clouds only, and the shapes are noisy. VisTracker [55] requires known object templates, hence we augment it with our reconstructed objects (denoted as †). Our method reconstructs the objects and tracks the poses accurately. (Purple balls indicate contact predictions.)

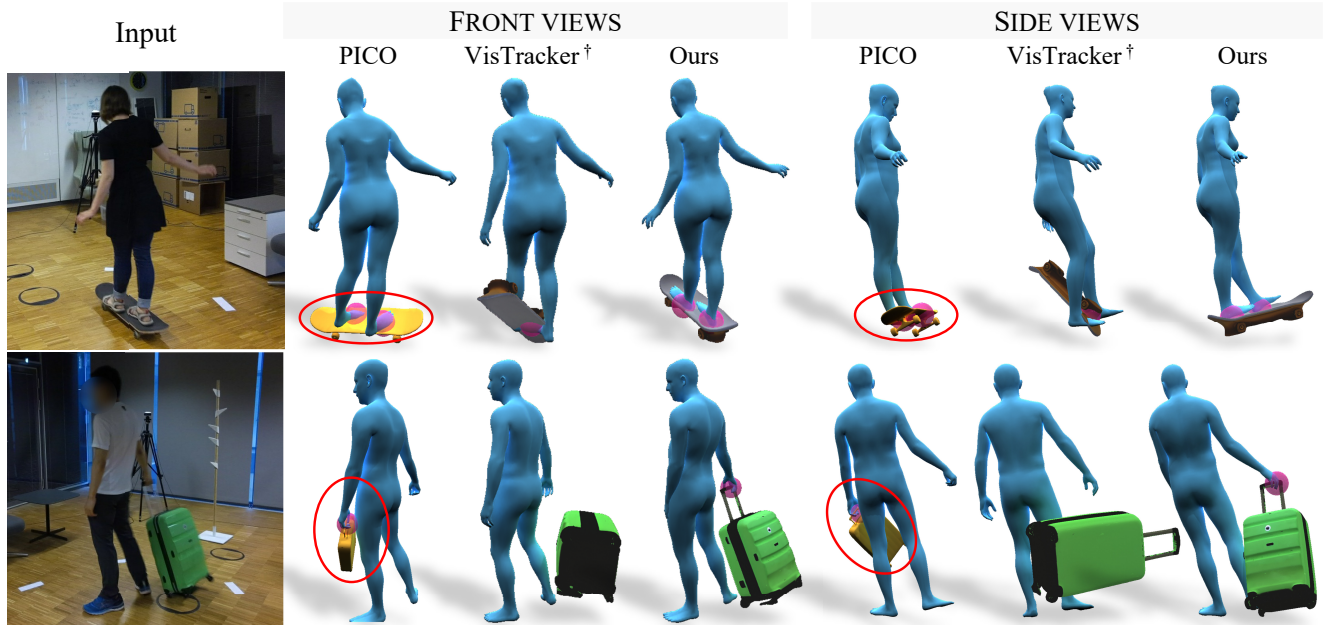


Figure 4. **Zero-shot generalization to unseen InterCap dataset** [18]. † Uses our reconstructed object meshes. Our method reconstructs the metric-scale object accurately and generalizes to unseen objects. (Purple balls indicate contact predictions.)

We test the models on the BEHAVE test set and unseen InterCap [18] test set, following the same split as prior works [10, 55]. Both BEHAVE and InterCap were captured in multi-view camera setup, and previous methods simply pick a fixed camera view for test regardless of the occlusion and view angles. Although this is the most general setting, it is far from a practical video recording setup. We hence se-

lect test views where the object is mostly visible in the first few frames, making the evaluation more suitable to downstream applications. In total 62 videos from BEHAVE and 22 videos from InterCap are selected for evaluation.

Evaluation Metrics. We report the chamfer distance (cm) between reconstructed and GT meshes of SMPL (CD-h), object (CD-o) and combined mesh (CD-c). Prior works

perform frame based [10, 27, 54, 56] with GT to remove the depth-scale ambiguity. This ignores the negative impact of temporally inconsistent scale or translation drift that frequently occurs in 4D reconstruction. Instead, to consider the world space translation, we align the first frame reconstruction to GT and apply the same transformation to the full video. For the first frame alignment, We utilize SMPL mesh only, instead of the combined human object mesh ([55]), as the reconstructed objects do not have the same topology as the GT mesh. We also report the acceleration error to measure the smoothness of the reconstructed motion. We define human acceleration error (Acc-h) as the mean per joint acceleration error against ground truth [23, 69] and object acceleration error (Acc-o) as the translation acceleration against GT.

4.1. Baseline Comparison

We compare against InterTrack [57] and VisTracker [55] on the BEHAVE test set in Tab. 1. All models have been trained with BEHAVE training set. Template-free approach, InterTrack, reconstructs human and object as 4D point cloud sequences normalized at each frame. Its lack of surface reconstruction and varying scale across frames makes it difficult for downstream applications. Furthermore, the translation from InterTrack is estimated using heuristics and 2D bounding boxes, leading to inconsistent global translations and thereby much higher errors than other methods under the 4D globally aligned setup (Tab. 1 row 1). VisTracker requires known object templates as input. In order to adapt to the considered setup where object information is unknown, we align our reconstructed object meshes with GT and augment VisTracker with the aligned object reconstructions. While producing consistent translation and smooth motion, VisTracker predicts less accurate results due to noisy pose and contact predictions. Our method, on the other hand, not only reconstructs the object meshes more accurately with metric scale, but also recovers the human and object poses coherently across the full video, outperforming prior methods by over 38% in terms of chamfer distance (CD-c). We also show some qualitative comparison in Fig. 3.

Method	CD-h↓	CD-o↓	CD-c↓	Acc-h↓	Acc-o↓
InterTrack	25.71	47.66	30.20	5.23	5.64
VisTracker	13.52	18.29	14.22	0.54	0.77
Ours	7.25	11.61	8.80	1.05	0.29

Table 1. **Evaluation results on BEHAVE [3] dataset** (unit: cm). Our method significantly outperforms previous instance-specific VisTracker [55] and category-specific InterTrack [11].

4.2. Zero-shot Generalization

We evaluate the zero-shot generalization ability of our method on the InterCap [18] test set and compare with

image based method PICO [10] and video based tracking methods InterTrack and VisTracker [55, 57]. All methods are not trained on InterCap. PICO is image based optimization method which is extremely computationally expensive (5min/image) to run on full videos hence we compare with it on key frames (3fps) only. PICO relies on predicted contacts on human body [42] to retrieve an object mesh and one-to-one contact correspondence between human and object vertices. Due to noisy human contact predictions from [42], its retrieval may result in wrong correspondence in the meshes such as swapped left and right (Fig. 4 row 2) or wrong contact location (Fig. 5 row 3), leading to large errors in both object pose and shape.

InterTrack and VisTracker are category or instance specific tracking methods, hence struggle to generalize to unseen instances or categories in InterCap. In contrast, our method is category agnostic and generalizes to novel instances and categories, see also the qualitative comparison in Fig. 4. We also test our method on in-the-wild internet videos, and results are shown in Fig. 1 and Fig. 5. Our method generalizes well to diverse object shapes, categories and interaction types. We show more results in Supp. video.

Method	CD-h↓	CD-o↓	CD-c↓	Acc-h↓	Acc-o↓
PICO*	5.15	27.63	87.73	-	-
Ours*	3.21	9.04	5.90	-	-
InterTrack	34.79	40.37	33.53	4.34	5.26
VisTracker	16.12	27.41	20.17	0.98	1.25
Ours	11.06	15.69	12.88	1.25	0.82

Table 2. **Zero-shot generalization to unseen InterCap [18] dataset** (unit: cm). *Denotes key-frames only, where acceleration metrics do not apply. Our method outperforms both image based method PICO [10] and video based tracking methods [55, 57].

4.3. Ablation Studies

We ablate the design choices of our method using a subset (24 videos, cover all objects) of the full BEHAVE [3] test set. We report chamfer and smoothness errors in Tab. 3.

Human and object initialization. We propose a dynamic pose hypothesis selection algorithm to obtain more robust object pose tracking using FoundationPose (FP [50]). We also align NLF [36] human predictions to UniDepth [32] depth estimation such that human and object are in the same metric-scale space. In Tab. 3, we compare our proposed initialization (row c) against the raw NLF predictions (w/o alignment) combined with FP in tracking (row a) or per-frame estimation (row b) mode. Our initialization is significantly better than raw NLF and FP results.

Contact reasoning model CoCoNet and training. We introduce CoCoNet to further refine our initialized human and object poses and reason about the contacts. In Tab. 3 we show that our CoCoNet (row e) improves our initial hu-



Figure 5. **Generalization to in-the-wild videos.** Prior methods predict noisy shape (InterTrack [57]), flipped object pose (VisTracker [55], [†] with our object reconstruction) or wrong contacts and object position (PICO [10]). Our method generalizes better overall. (Purple balls indicate contact predictions.)

Method	CD-h \downarrow	CD-o \downarrow	CD-c \downarrow	Acc-h \downarrow	Acc-o \downarrow
a. Raw NLF + FP tracking	11.53	1565.42	405.13	3.06	4.34
b. Raw NLF + FP pose est.	11.53	40.54	13.02	3.06	9.26
c. Our init. NLF + FP	7.81	16.85	10.79	2.21	8.36
d. Our init. + ref. w/o align	8.01	13.55	9.95	2.08	3.74
e. Our init. + ref. w/ align	7.01	11.59	8.62	1.75	3.78
f. Our full model	8.41	11.57	9.35	1.06	0.38

Table 3. **Ablation studies.** Our proposed initialization (c) is better than running vanilla (a, b) NLF [36] and FoundationPose (FP [50]). Our contact reasoning model trained with the proposed alignment (e) further improves the accuracy. Joint optimization (f) improves smoothness and contact consistency (see Fig. 6).

man and object reconstructions (row c). To ensure consistency between the ground-truth poses from the datasets and the initialized metric-scaled human, object, and monocular depth, we propose to align them for training. To ablate this training strategy, we then train a model without our alignment (row d) which yields even worse results than the initialization on human, since the model is tasked for an ill-posed problem: predicting the correct pose updates for the misaligned human pose and monocular depth. This highlights the importance of our CoCoNet and training strategy.

Contact based joint optimization. Our CoCoNet predicts contacts which is then used to further optimize the output poses from our CoCoNet to satisfy physical constraints. Compared to the initial prediction from CoCoNet (Tab. 3 e), our joint optimization improves the motion smoothness and coherency of the contacts. We show two examples in Fig. 6.

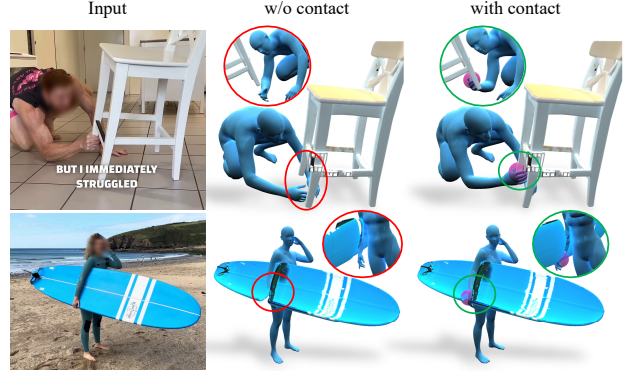


Figure 6. **Importance of contacts.** Without our contact-aware optimization, the model does not properly handle the fine-grained hand-object interaction, leading to floating object or penetration errors. (Purple balls indicate contact predictions.)

Without optimization, the model is not aware of the intricate contact points on the object, leading to artifacts such as penetration or floating objects. Our optimization refines the object and hand poses, leading to smoother and more coherent reconstruction (Tab. 3 between f and e).

Oracle study. The primary focus of this paper is to develop a general method for RGB based 4D reconstruction without any object shape or depth information as inputs. We test the performance of our method when their privileged information is given in Tab. 4. It can be seen that ground truth object shape or depth improves slightly the object reconstruction and combining both achieves the most boost. Our base model designed for RGB input is close to the upper bound with oracle GT information.

Method	CD-h \downarrow	CD-o \downarrow	CD-c \downarrow	Acc-h \downarrow	Acc-o \downarrow
Ours	8.41	11.57	9.35	1.06	0.38
+GT mesh	8.05	9.26	8.18	1.03	0.32
+GT dmap	7.50	11.25	8.78	0.94	0.35
+GT mesh&dmap	7.23	7.78	7.20	0.92	0.27

Table 4. **Oracle study.** Trained on estimated depth, our model also allows input with ground truth depth or object mesh and achieves slightly better results.

5. Conclusion

We present CARI4D, a category agnostic method to reconstruct 4D human object interaction from monocular RGB video. Our key idea is to design a framework that aligns the predictions from foundation models to obtain a robust initialization followed by learned contact reasoning and interaction refinement. We first perform coarse to fine scale estimation to recover metric-scale for the object and then introduce pose hypothesis selection for robust object pose tracking. We then train our CoCoNet that predicts hand contacts and refines the initial interaction poses which is then used to jointly optimize the poses together with contacts. We evaluate CARI4D on BEHAVE and unseen InterCap datasets, achieving over 36% improvement in Chamfer distance for

both in-distribution and zero-shot settings. Ablations confirm the effectiveness of our pose selection, CoCoNet, and other design choices. CARI4D also generalizes well to in-the-wild videos with diverse objects and interactions. Code and pretrained models will be released.

References

- [1] <https://github.com/cmu-perceptual-computing-lab/openpose>. 1
- [2] Stability AI. Stable video diffusion: A novel approach to image-to-video generation. *arXiv preprint arXiv:2308.09592*, 2023. Available at <https://github.com/Stability-AI/generative-models>. 5
- [3] Bharat Lal Bhatnagar, Xianghui Xie, Ilya Petrov, Cristian Sminchisescu, Christian Theobalt, and Gerard Pons-Moll. Behave: Dataset and method for tracking human object interactions. In *IEEE Conference on Computer Vision and Pattern Recognition (CVPR)*, 2022. 3, 5, 6, 7, 1
- [4] Michael J. Black, Priyanka Patel, Joachim Tesch, and Jinlong Yang. BEDLAM: A synthetic dataset of bodies exhibiting detailed lifelike animated motion. In *Proceedings IEEE/CVF Conf. on Computer Vision and Pattern Recognition (CVPR)*, pages 8726–8737, 2023. 2
- [5] Aleksei Bochkovskii, Amaël Delaunoy, Hugo Germain, Marcel Santos, Yichao Zhou, Stephan R. Richter, and Vladlen Koltun. Depth pro: Sharp monocular metric depth in less than a second. In *International Conference on Representation Learning (ICLR)*, 2025. 2
- [6] Derek Bradley, Tiberiu Popa, Alla Sheffer, Wolfgang Heidrich, and Tamy Boubekeur. Markerless garment capture. *ACM Trans. Graph.*, 27(3):1–9, 2008. 2
- [7] Zhongang Cai, Wanqi Yin, Ailing Zeng, Chen Wei, Qingping Sun, Yanjun Wang, Hui En Pang, Haiyi Mei, Mingyuan Zhang, Lei Zhang, Chen Change Loy, Lei Yang, and Ziwei Liu. SMPLer-X: Scaling up expressive human pose and shape estimation. In *Advances in Neural Information Processing Systems (NeurIPS) — Datasets and Benchmarks Track*, 2023. 2
- [8] Sili Chen, Hengkai Guo, Shengnan Zhu, Feihu Zhang, Zilong Huang, Jiashi Feng, and Bingyi Kang. Video depth anything: Consistent depth estimation for super-long videos. *arXiv preprint arXiv:2501.12375*, 2025. 2
- [9] Alvaro Collet, Ming Chuang, Pat Sweeney, Don Gillett, Dennis Evseev, David Calabrese, Hugues Hoppe, Adam Kirk, and Steve Sullivan. High-quality streamable free-viewpoint video. *ACM Trans. Graph.*, 34(4), 2015. 2
- [10] Alpár Cseke, Shashank Tripathi, Sai Kumar Dwivedi, Arjun Lakshmipathy, Agniv Chatterjee, Michael J. Black, and Dimitrios Tzionas. PICO: Reconstructing 3D people in contact with objects. In *Proceedings of the IEEE/CVF Conference on Computer Vision and Pattern Recognition (CVPR)*, pages 1783–1794, 2025. 2, 3, 6, 7, 8
- [11] Sai Kumar Dwivedi, Dimitrije Antić, Shashank Tripathi, Omid Taheri, Cordelia Schmid, Michael J. Black, and Dimitrios Tzionas. InteractVLM: 3D interaction reasoning from 2D foundational models. In *Proceedings of the IEEE/CVF Conference on Computer Vision and Pattern Recognition (CVPR)*, 2025. 3, 7
- [12] Zicong Fan, Maria Parelli, Maria Eleni Kadoglou, Muhammed Kocabas, Xu Chen, Michael J Black, and Otmar Hilliges. HOLD: Category-agnostic 3d reconstruction of interacting hands and objects from video. In *Proceedings of the IEEE/CVF Conference on Computer Vision and Pattern Recognition*, pages 494–504, 2024. 3
- [13] Shubham Goel, Georgios Pavlakos, Jathushan Rajasegaran, Angjoo Kanazawa, and Jitendra Malik. Humans in 4D: Reconstructing and tracking humans with transformers. In *ICCV*, 2023. 2
- [14] Chen Guo, Tianjian Jiang, Manuel Kaufmann, Chengwei Zheng, Julien Valentin, Jie Song, and Otmar Hilliges. Reloo: Reconstructing humans dressed in loose garments from monocular video in the wild. In *European conference on computer vision (ECCV)*, 2024. 2
- [15] Chen Guo, Junxuan Li, Yash Kant, Yaser Sheikh, Shunsuke Saito, and Chen Cao. Vid2avatar-pro: Authentic avatar from videos in the wild via universal prior. In *Proceedings of the IEEE/CVF Conference on Computer Vision and Pattern Recognition (CVPR)*, 2025. 2
- [16] Yana Hasson, Gül Varol, Dimitrios Tzionas, Igor Kalevatykh, Michael J. Black, Ivan Laptev, and Cordelia Schmid. Learning joint reconstruction of hands and manipulated objects. In *CVPR*, 2019. 3
- [17] Yana Hasson, Bugra Tekin, Federica Bogo, Ivan Laptev, Marc Pollefeys, and Cordelia Schmid. Leveraging photometric consistency over time for sparsely supervised hand-object reconstruction. In *CVPR*, 2020. 3
- [18] Yinghao Huang, Omid Taheri, Michael J. Black, and Dimitrios Tzionas. InterCap: Joint markerless 3D tracking of humans and objects in interaction. In *German Conference on Pattern Recognition (GCPR)*, pages 281–299. Springer, 2022. 3, 6, 7
- [19] Chaofan Huo, Ye Shi, and Jingya Wang. Monocular human-object reconstruction in the wild. In *Proceedings of the 32nd ACM International Conference on Multimedia*, page 5547–5555, New York, NY, USA, 2024. Association for Computing Machinery. 3
- [20] Hsuan I Ho, Jie Song, and Otmar Hilliges. Sith: Single-view textured human reconstruction with image-conditioned diffusion. In *Proceedings of the IEEE/CVF Conference on Computer Vision and Pattern Recognition (CVPR)*, pages 538–549, 2024. 2
- [21] Catalin Ionescu, Dragos Papava, Vlad Olaru, and Cristian Sminchisescu. Human3.6m: Large scale datasets and predictive methods for 3d human sensing in natural environments. *IEEE Transactions on Pattern Analysis and Machine Intelligence*, 36(7):1325–1339, 2014. 2
- [22] Hanbyul Joo, Tomas Simon, and Yaser Sheikh. Total capture: A 3d deformation model for tracking faces, hands, and bodies. In *2018 IEEE/CVF Conference on Computer Vision and Pattern Recognition*, pages 8320–8329, 2018. 2
- [23] Jiefeng Li, Jinkun Cao, Haotian Zhang, Davis Rempe, Jan Kautz, Umar Iqbal, and Ye Yuan. Genmo: Genera-

- tive models for human motion synthesis. *arXiv preprint arXiv:2505.01425*, 2025. 2, 7
- [24] Yunze Liu, Yun Liu, Che Jiang, Kangbo Lyu, Weikang Wan, Hao Shen, Boqiang Liang, Zhoujie Fu, He Wang, and Li Yi. Hoi4d: A 4d egocentric dataset for category-level human-object interaction. In *Proceedings of the IEEE/CVF Conference on Computer Vision and Pattern Recognition (CVPR)*, pages 21013–21022, 2022. 3
- [25] Matthew Loper, Naureen Mahmood, Javier Romero, Gerard Pons-Moll, and Michael J. Black. SMPL: A skinned multi-person linear model. In *ACM Transactions on Graphics*. ACM, 2015. 3
- [26] Marko Mihajlovic, Siwei Zhang, Gen Li, Kaifeng Zhao, Lea Müller, and Siyu Tang. VolumetricSMPL: A neural volumetric body model for efficient interactions, contacts, and collisions. In *Proceedings of the IEEE/CVF International Conference on Computer Vision (ICCV)*, 2025. 5, 1
- [27] Hyeongjin Nam, Daniel Sungho Jung, Gyeongseok Moon, and Kyoung Mu Lee. Joint reconstruction of 3d human and object via contact-based refinement transformer. In *Proceedings of the IEEE/CVF Conference on Computer Vision and Pattern Recognition*, 2024. 3, 7
- [28] Maxime Oquab, Timothée Darcet, Théo Moutakanni, Huy Vo, Marc Szafranec, Vasil Khalidov, Pierre Fernandez, Daniel Haziza, Francisco Massa, Alaaeldin El-Nouby, Mahmoud Assran, Nicolas Ballas, Wojciech Galuba, Russell Howes, Po-Yao Huang, Shang-Wen Li, Ishan Misra, Michael Rabbat, Vasu Sharma, Gabriel Synnaeve, Hu Xu, Hervé Jegou, Julien Mairal, Patrick Labatut, Armand Joulin, and Piotr Bojanowski. Dinov2: Learning robust visual features without supervision, 2024. 5, 1
- [29] Priyanka Patel, Chun-Hao P. Huang, Joachim Tesch, David T. Hoffmann, Shashank Tripathi, and Michael J. Black. AGORA: Avatars in geography optimized for regression analysis. In *2021 IEEE/CVF Conference on Computer Vision and Pattern Recognition (CVPR)*, page 13463–13473, 2021. 2
- [30] Georgios Pavlakos, Dandan Shan, Ilija Radosavovic, Angjoo Kanazawa, David Fouhey, and Jitendra Malik. Reconstructing hands in 3D with transformers. In *CVPR*, 2024. 2
- [31] Luigi Piccinelli, Yung-Hsu Yang, Christos Sakaridis, Mattia Segu, Siyuan Li, Luc Van Gool, and Fisher Yu. UniDepth: Universal monocular metric depth estimation. In *Proceedings of the IEEE/CVF Conference on Computer Vision and Pattern Recognition (CVPR)*, 2024. 2, 3, 4
- [32] Luigi Piccinelli, Christos Sakaridis, Yung-Hsu Yang, Mattia Segu, Siyuan Li, Wim Abbeloos, and Luc Van Gool. UniDepthV2: Universal monocular metric depth estimation made simpler, 2025. 2, 3, 5, 7
- [33] Rolandos Alexandros Potamias, Jinglei Zhang, Jiankang Deng, and Stefanos Zafeiriou. Wilor: End-to-end 3d hand localization and reconstruction in-the-wild, 2024. 2
- [34] René Ranftl, Katrin Lasinger, David Hafner, Konrad Schindler, and Vladlen Koltun. Towards robust monocular depth estimation: Mixing datasets for zero-shot cross-dataset transfer. *IEEE Transactions on Pattern Analysis and Machine Intelligence*, 44(3), 2022. 2, 5
- [35] Javier Romero, Dimitrios Tzionas, and Michael J. Black. Embodied hands: Modeling and capturing hands and bodies together. *ACM Transactions on Graphics, (Proc. SIGGRAPH Asia)*, 36(6), 2017. 3
- [36] István Sárárdi and Gerard Pons-Moll. Neural localizer fields for continuous 3d human pose and shape estimation. 2024. 2, 3, 4, 5, 7, 8
- [37] Konstantin Sofiiuk, Ilia Petrov, Olga Barinova, and Anton Konushin. f-brs: Rethinking backpropagating refinement for interactive segmentation. In *Proceedings of the IEEE/CVF Conference on Computer Vision and Pattern Recognition*, pages 8623–8632, 2020. 3
- [38] Zhuo Su, Lan Xu, Dawei Zhong, Zhong Li, Fan Deng, Shuxue Quan, and Lu Fang. Robustfusion: Robust volumetric performance reconstruction under human-object interactions from monocular RGBD stream. *CoRR*, abs/2104.14837, 2021. 3
- [39] Guoxing Sun, Xin Chen, Yizhang Chen, Anqi Pang, Pei Lin, Yuheng Jiang, Lan Xu, Jingya Wang, and Jingyi Yu. Neural free-viewpoint performance rendering under complex human-object interactions. In *Proceedings of the 29th ACM International Conference on Multimedia*, 2021. 3
- [40] Tencent Hunyuan3D Team. Hunyuan3d 2.0: Scaling diffusion models for high resolution textured 3d assets generation, 2025. 2, 3
- [41] Dmitry Tochilkin, David Pankratz, Zexiang Liu, Zixuan Huang, Adam Letts, Yangguang Li, Ding Liang, Christian Laforte, Varun Jampani, and Yan-Pei Cao. Triposr: Fast 3d object reconstruction from a single image. *arXiv preprint arXiv:2403.02151*, 2024. 2
- [42] Shashank Tripathi, Agniv Chatterjee, Jean-Claude Passy, Hongwei Yi, Dimitrios Tzionas, and Michael J. Black. DECO: Dense estimation of 3D human-scene contact in the wild. In *Proceedings of the IEEE/CVF International Conference on Computer Vision (ICCV)*, pages 8001–8013, 2023. 3, 7
- [43] Vikram Voleti, Chun-Han Yao, Mark Boss, Adam Letts, David Pankratz, Dmitrii Tochilkin, Christian Laforte, Robin Rombach, and Varun Jampani. SV3D: Novel multi-view synthesis and 3D generation from a single image using latent video diffusion. In *Proceedings of the European Conference on Computer Vision (ECCV)*, 2024. 2, 1
- [44] He Wang, Srinath Sridhar, Jingwei Huang, Julien Valentin, Shuran Song, and Leonidas J Guibas. Normalized object coordinate space for category-level 6d object pose and size estimation. In *Proceedings of the IEEE/CVF conference on computer vision and pattern recognition*, pages 2642–2651, 2019. 5
- [45] Jianyuan Wang, Minghao Chen, Nikita Karaev, Andrea Vedaldi, Christian Rupprecht, and David Novotny. Vggt: Visual geometry grounded transformer. In *Proceedings of the IEEE/CVF Conference on Computer Vision and Pattern Recognition*, 2025. 2
- [46] Ruicheng Wang, Sicheng Xu, Cassie Dai, Jianfeng Xiang, Yu Deng, Xin Tong, and Jiaolong Yang. Moge: Unlocking accurate monocular geometry estimation for open-domain images with optimal training supervision. In *Proceedings of*

- the IEEE/CVF Conference on Computer Vision and Pattern Recognition (CVPR)*, pages 5261–5271, 2025. Oral. 2
- [47] Ruicheng Wang, Sicheng Xu, Yue Dong, Yu Deng, Jianfeng Xiang, Zelong Lv, Guangzhong Sun, Xin Tong, and Jiaolong Yang. Moge-2: Accurate monocular geometry with metric scale and sharp details. *arXiv preprint*, 2025. 2
- [48] Shuzhe Wang, Vincent Leroy, Yohann Cabon, Boris Chidlovskii, and Jerome Revaud. Dust3r: Geometric 3d vision made easy. In *CVPR*, 2024. 2
- [49] Bowen Wen, Jonathan Tremblay, Valts Blukis, Stephen Tyree, Thomas Müller, Alex Evans, Dieter Fox, Jan Kautz, and Stan Birchfield. BundleSDF: Neural 6-DoF tracking and 3D reconstruction of unknown objects. In *CVPR*, 2023. 2
- [50] Bowen Wen, Wei Yang, Jan Kautz, and Stan Birchfield. FoundationPose: Unified 6D Pose Estimation and Tracking of Novel Objects. In *CVPR*, 2024. 2, 3, 5, 7, 8
- [51] Boran Wen, Dingbang Huang, Zichen Zhang, Jiahong Zhou, Jianbin Deng, Jingyu Gong, Yulong Chen, Lizhuang Ma, and Yong-Lu Li. Reconstructing in-the-wild open-vocabulary human-object interactions, 2025. 3
- [52] Zhenzhen Weng and Serena Yeung. Holistic 3d human and scene mesh estimation from single view images. *arXiv preprint arXiv:2012.01591*, 2020. 3
- [53] Jianfeng Xiang, Zelong Lv, Sicheng Xu, Yu Deng, Ruicheng Wang, Bowen Zhang, Dong Chen, Xin Tong, and Jiaolong Yang. Structured 3d latents for scalable and versatile 3d generation. In *Proceedings of the IEEE/CVF Conference on Computer Vision and Pattern Recognition (CVPR)*, 2025. Spotlight. 2
- [54] Xianghui Xie, Bharat Lal Bhatnagar, and Gerard Pons-Moll. Chore: Contact, human and object reconstruction from a single rgb image. In *European Conference on Computer Vision (ECCV)*. Springer, 2022. 3, 5, 7
- [55] Xianghui Xie, Bharat Lal Bhatnagar, and Gerard Pons-Moll. Visibility aware human-object interaction tracking from single rgb camera. In *IEEE Conference on Computer Vision and Pattern Recognition (CVPR)*, 2023. 2, 3, 6, 7, 8
- [56] Xianghui Xie, Bharat Lal Bhatnagar, Jan Eric Lenssen, and Gerard Pons-Moll. Template free reconstruction of human-object interaction with procedural interaction generation. In *IEEE Conference on Computer Vision and Pattern Recognition (CVPR)*, 2024. 2, 3, 7
- [57] Xianghui Xie, Jan Eric Lenssen, and Gerard Pons-Moll. Intertrack: Tracking human object interaction without object templates. 2024. 2, 3, 6, 7, 8
- [58] Xianghui Xie, Xi Wang, Nikos Athanasiou, Bharat Lal Bhatnagar, Chun-Hao P. Huang, Kaichun Mo, Hao Chen, Xia Jia, Zerui Zhang, Liangxian Cui, Xiao Lin, Bingqiao Qian, Jie Xiao, Wenfei Yang, Hyeongjin Nam, Daniel Sungho Jung, Kihoon Kim, Kyoung Mu Lee, Otmar Hilliges, and Gerard Pons-Moll. RHOBIN Challenge: Reconstruction of human object interaction. *arXiv preprint arXiv:2401.04143*, 2024. 3
- [59] Xianghui Xie, Chuhang Zou, Meher Gitika Karumuri, Jan Eric Lenssen, and Gerard Pons-Moll. Mvbench: Comprehensive benchmark for multi-view generation models, 2025. 2
- [60] Yuxuan Xue, Xianghui Xie, Riccardo Marin, and Gerard Pons-Moll. Gen-3diffusion: Realistic image-to-3d generation via 2d & 3d diffusion synergy, 2024. 2
- [61] Yuxuan Xue, Xianghui Xie, Riccardo Marin, and Gerard Pons-Moll. Human 3diffusion: Realistic avatar creation via explicit 3d consistent diffusion models. In *Arxiv*, 2024. 2
- [62] Yuxuan Xue, Xianghui Xie, Margaret Kostyrko, and Gerard Pons-Moll. Infinihuman: Infinite 3d human creation with precise control. 2025. 2
- [63] Pradyumna Yalandur-Muralidhar, Yuxuan Xue, Xianghui Xie, Margaret Kostyrko, and Gerard Pons-Moll. Physic: Physically plausible 3d human-scene interaction and contact from a single image. In *ACM SIGGRAPH Asia*, 2025. 3
- [64] Lixin Yang, Xinyu Zhan, Kailin Li, Wenqiang Xu, Jiefeng Li, and Cewu Lu. CPF: Learning a contact potential field to model the hand-object interaction. In *ICCV*, 2021. 3
- [65] Lihe Yang, Bingyi Kang, Zilong Huang, Xiaogang Xu, Jiashi Feng, and Hengshuang Zhao. Depth anything: Unleashing the power of large-scale unlabeled data. In *Proceedings of the IEEE/CVF Conference on Computer Vision and Pattern Recognition (CVPR)*, 2024. *arXiv preprint arXiv:2401.10891*. 2
- [66] Yufei Ye, Poorvi Hebbar, Abhinav Gupta, and Shubham Tulsiani. Diffusion-guided reconstruction of everyday hand-object interaction clips. In *ICCV*, 2023. 3
- [67] Yufei Ye, Abhinav Gupta, Kris Kitani, and Shubham Tulsiani. G-hop: Generative hand-object prior for interaction reconstruction and grasp synthesis. In *CVPR*, 2024. 3
- [68] Ye Yuan, Umar Iqbal, Pavlo Molchanov, Kris Kitani, and Jan Kautz. Glamr: Global occlusion-aware human mesh recovery with dynamic cameras. In *Proceedings of the IEEE/CVF Conference on Computer Vision and Pattern Recognition (CVPR)*, 2022. 2
- [69] Ailing Zeng, Lei Yang, Xuan Ju, Jiefeng Li, Jianyi Wang, and Qiang Xu. Smoothnet: A plug-and-play network for refining human poses in videos. In *European Conference on Computer Vision*. Springer, 2022. 7
- [70] Juze Zhang, Haimin Luo, Hongdi Yang, Xinru Xu, Qianyang Wu, Ye Shi, Jingyi Yu, Lan Xu, and Jingya Wang. Neuraldome: A neural modeling pipeline on multi-view human-object interactions. In *CVPR*, 2023. 3, 5, 1
- [71] Juze Zhang, Jingyan Zhang, Zining Song, Zhanhe Shi, Chengfeng Zhao, Ye Shi, Jingyi Yu, Lan Xu, and Jingya Wang. Hoi-m3: Capture multiple humans and objects interaction within contextual environment. In *CVPR*, 2024. 3
- [72] Jinglei Zhang, Jiankang Deng, Chao Ma, and Rolandos Alexandros Potamias. Hawor: World-space hand motion reconstruction from egocentric videos. *arXiv preprint arXiv:2501.02973*, 2025. 2
- [73] Jason Y. Zhang, Sam PePOSE, Hanbyul Joo, Deva Ramanan, Jitendra Malik, and Angjoo Kanazawa. Perceiving 3d human-object spatial arrangements from a single image in the wild. In *European Conference on Computer Vision (ECCV)*, 2020. 3, 5, 1
- [74] Longwen Zhang, Ziyu Wang, Qixuan Zhang, Qiwei Qiu, Anqi Pang, Haoran Jiang, Wei Yang, Lan Xu, and Jingyi Yu.

Clay: A controllable large-scale generative model for creating high-quality 3d assets. *ACM Transactions on Graphics (TOG)*, 43(4):1–20, 2024. [2](#)

- [75] Chengfeng Zhao, Juze Zhang, Jiashen Du, Ziwei Shan, Junye Wang, Jingyi Yu, Jingya Wang, and Lan Xu. I'm hoi: Inertia-aware monocular capture of 3d human-object interactions. In *Proceedings of the IEEE/CVF Conference on Computer Vision and Pattern Recognition*, pages 729–741, 2024.

[3](#)

CARI4D: Category Agnostic 4D Reconstruction of Human-Object Interaction

Supplementary Material

In this supplementary, we discuss in more details about our CoCoNet architecture, joint optimization and runtime performance. We then discuss limitations and failure cases. Please refer to our supplementary video for 4D reconstruction results and baseline comparisons.

6. Implementation Details

We detail our implementations in this section. Note that our code and pretrained models will be fully released with detailed documentation to enable reproduction of our results.

6.1. CoCoNet Details

Network architecture. We plot the architecture diagram of our CoCoNet in Fig. 7. We adopt DINOv2 [28] as our image encoder and keep the base DINO for RGB image frozen while the small DINO model for xyz map and mask is fine tuned. We replace the first convolution layer in DINOv2 small to consume five channels (xyz + human object masks) instead of three RGB channels and finetune it end to end with other network layers. The attention block is spatiotemporal attention module similar to SV3D [43]. Specifically, given feature grid of shape (b, t, d, h, w) , we first reshape and perform spatial attention on feature (bt, hw, d) to obtain \mathbf{F}_s , followed by a temporal attention on feature (bhw, t, d) to obtain \mathbf{F}_t . We then blend spatial feature \mathbf{F}_s and temporal feature \mathbf{F}_t with a learnable factor $\alpha \in [0, 1]$: $\mathbf{F} = (1 - \alpha)\mathbf{F}_s + \alpha\mathbf{F}_t$. We use two spatiotemporal attention blocks in our network and temporal window size is $t = 96$. Following the spatiotemporal attention are five MLP heads that regress delta updates of object rotation $\Delta\mathbf{R} \in \mathbb{R}^6$, object translation $\Delta\mathbf{t}^o \in \mathbb{R}^3$, SMPL pose $\Delta\theta \in \mathbb{R}^{144}$, SMPL shape $\Delta\beta \in \mathbb{R}^{10}$, and SMPL translation $\Delta\mathbf{t}^h \in \mathbb{R}^3$.

Training details. We train our model on BEHAVE [3] and HODome [70] dataset following the data preprocessing discussed in Sec. 3.3. We use AdamW optimizer with a learning rate of 1e-4 and an effective batch size of 16 for 38k steps. The training process takes about 38 hours on $8 \times \text{A100@80GB}$ GPUs.

6.2. Joint Optimization

We discuss in more details the objective function for our contact aware joint optimization (Sec. 3.4). Given a sequence of refined human-object poses $\{\mathcal{H}_i, \mathcal{O}_i\}_{i=1}^N$ and binary hand contact labels $\{\mathbf{c}_i\}_{i=1}^N$ predicted by our CoCoNet, we aim at improving its contact realism and avoiding penetration via optimizing the pose parameters

$\{\mathcal{H}_i, \mathcal{O}_i\}_{i=1}^N$. The overall objective function is defined as:

$$L = \lambda_c L_c + \lambda_{j2d} L_{j2d} + \lambda_m L_m + \lambda_{pen} L_{pen} + \lambda_{acc} L_{acc} \quad (3)$$

where $L_c, L_{j2d}, L_m, L_{pen}, L_{acc}$ are the contact loss, 2D body joint reprojection loss, object mask loss, penetration loss and acceleration loss respectively.

The contact loss L_c penalizes large distances between hand and object when there is contact: $L_c = \sum_i d(\mathbf{J}_i^h, \mathbf{O}'_i) \cdot \mathbf{c}_i$, where $d(\cdot, \cdot)$ computes the closest distance from two hand joints $\mathbf{J}_i^h \in \mathbb{R}^6$ to the posed object points \mathbf{O}'_i .

The 2D joint projection loss L_{j2d} minimizes the distance between projected 2D joints $\pi(\mathbf{J}(\mathbf{H}_i))$ and detected 2D joints $\hat{\mathbf{J}}_i$ from input image using openpose [1]: $L_{j2d} = \sum_i \|\hat{\mathbf{J}}_i - \pi(\mathbf{J}(\mathbf{H}_i))\|_2^2$, where $\mathbf{J}(\cdot)$ regresses the 3D body joints from SMPL mesh \mathbf{H}_i and $\pi(\cdot)$ projects the 3D joints to 2D image.

The 2D object mask loss L_m is occlusion aware and defined as: $L_m = \sum (M - I \circ S)^2$, where M is the input object mask, I is a non-occlusion indicator (1 if pixel belongs only to this object, 0 else) and S is the rendered object silhouette. The non-occlusion indicator is derived from human and object masks. The human and object masks may have overlap regions due to imperfect segmentation. To address this, pixels that belong only to object mask are assigned value 1 for the non-occlusion indicator. This avoids computing loss on regions where the object is occluded, see illustration in PHOSA [73].

We define the penetration loss using Volumetric SMPL [26] which learns a function Φ_{SMPL} that predicts a signed distance given a query point $q \in \mathbb{R}^3$, formally: $\Phi_{\text{SMPL}} : \mathbb{R}^3 \mapsto \mathbb{R}$. The penetration loss is hence defined as: $L_{pen} = \sum_i \sum_{q \in \mathcal{O}'_i} \text{ReLU}(-\Phi_{\text{SMPL}}(q))^2$. In practice we sample 6000 points on the object mesh surface as query points to compute the penetration loss.

The acceleration loss L_{acc} avoids large jitters by pushing the acceleration to be zero. In general: $L_{acc} = \|\mathbf{x}_i - 2\mathbf{x}_{i-1} + \mathbf{x}_{i-2}\|_2^2$, here \mathbf{x} includes 3D human body joints $\mathbf{J}(\mathbf{H})$ and object poses.

The loss weights are $\lambda_c = 200, \lambda_{j2d} = 0.03, \lambda_m = 0.002, \lambda_{pen} = 2.0$ and we use $\lambda_{acc} = 600$ for human body joints, $\lambda_{acc} = 1000$ for object poses. We use Adam optimizer with linear learning rate decay (start with 1e-3 learning rate) to optimize the parameters for 3000 steps. For efficiency we add penetration loss only in the last 1200 steps.

6.3. Runtime Performance

We report the average runtime of different methods to finish processing a video sequence of 300 frames using

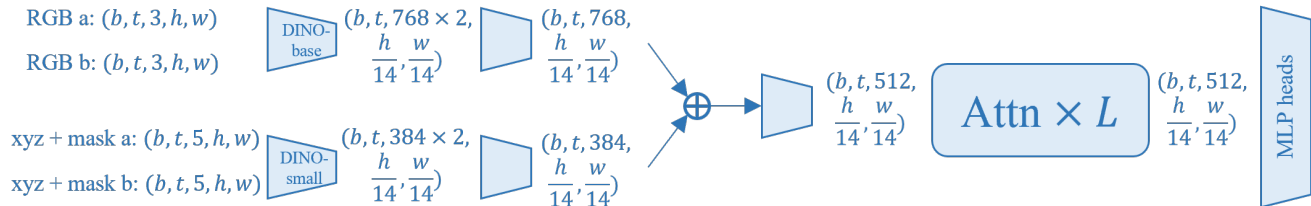


Figure 7. **CoCoNet architecture**. Here b, t, h, w denote batch size, temporal window size, image height and width respectively. We follow a render-and-compare paradigm, hence RGB a and RGB b denote the image from input observation and rendering respectively, same for xyz map and mask (human and object stacked together).

one A100@80GB GPU in Tab. 5. Image based approach PICO [10] requires the longest time as it optimizes one image each time and each optimization takes almost five minutes to finish. Video based methods InterTrack [57] and VisTracker [55] are faster as they leverage temporal cues and process multiple frames in parallel. However, they are still lower than our method due to complex multi-stage optimization (VisTracker [55]) or diffusion sampling process (InterTrack [57]). Our method achieves the fastest runtime while still producing the most accurate results.

Method	PICO	InterTrack	VisTracker	Ours
Runtime (min) ↓	1560	198	118	45

Table 5. **Average runtime (minutes)** to process one video of 300 frames. Our method is much faster than baselines while being more accurate.

7. Limitation and Future

As the first step towards category agnostic 4D interaction reconstruction, our method shows strong generalization performance to in-the-wild videos, yet there are still some limitations. We show two typical failure cases in Fig. 8.

First, our method primarily targets full-body human-object interaction; consequently, it does not explicitly regress detailed finger articulations. This limitation becomes particularly pronounced during interactions involving small-scale objects or those requiring fine-grained manipulation, such as grasping plates (Fig. 8, top row). In such scenarios, the absence of precise finger kinematics results in physically implausible interaction configurations, even when the full body pose is accurate. To bridge this gap, future iterations could integrate specialized hand pose estimators [30, 33, 72]. By solving for the hand parameters separately and fusing them with the full-body kinematic chain via optimization, one could achieve a holistic reconstruction that respects both macro-level body dynamics and micro-level contact physics.

Second, our method relies on FoundationPose [50] for object pose initialization, subsequently refining these estimates using human interaction cues and visual evidence. A



Figure 8. **Failure case examples**. Our method focuses on full body interaction and the detailed hand poses are not handled, which can be important for fine-grained object manipulation task (top row). Our method thus failed to reconstruct realistic finger poses for holding the plate. Under highly dynamic motion and extreme occlusion (bottom row), FoundationPose predicts flipped object pose for initialization. Such large rotation error is not able to be corrected by our refinement process in subsequent steps, leading to inaccurate reconstruction in the end.

notable dependency bottleneck arises when the initializer fails significantly. FoundationPose can occasionally predict flipped 180-degree poses under conditions of rapid motion or severe occlusion (Fig. 8, bottom row). In these instances, the error magnitude is often too large for our refinement network to correct. A promising direction is the incorporation of temporal priors and motion infilling, similar to strategies employed in VisTracker [55] or GLAMR [68]. By leveraging information from visible frames to hallucinate motion in occluded segments, we can enforce temporal smoothness and recover from initialization failures.